J Artif Organs (2007) 10:96–103
DOI 10.1007/s10047-006-0365-9

ORIGINAL ARTICLE

Yos S. Morsi, PhD · William W. Yang, PhD
Cynthia S. Wong, PhD · Subrat Das, PhD

Transient fluid–structure coupling for simulation of a trileaflet heart valve using weak coupling

Abstract In this article, a three-dimensional transient numerical approach coupled with fluid–structure interaction for the modeling of an aortic trileaflet heart valve at the initial opening stage is presented. An arbitrary Lagrangian–Eulerian kinematical description together with an appropriate fluid grid was used for the coupling strategy with the structural domain. The fluid dynamics and the structure aspects of the problem were analyzed for various Reynolds numbers and times. The fluid flow predictions indicated that at the initial leaflet opening stage a circulation zone was formed immediately downstream of the leaflet tip and propagated outward as time increased. Moreover, the maximum wall shear stress in the vertical direction of the leaflet was found to be located near the bottom of the leaflet, and its value decreased sharply toward the tip. In the horizontal cross section of the leaflet, the maximum wall shear stresses were found to be located near the sides of the leaflet.

Key words Trileaflet heart valve · Computational fluid dynamics · Fluid–structure interaction · Arbitrary Lagrangian–Eulerian method · Wall shear stress

Introduction

Prosthetic heart valves are commonly used to replace natural heart valves and are also widely adapted in ventricular assist devices (VAD) as well as in total artificial hearts (TAH). It is well understood that the clinical success of any valve design is based on many factors, including fluid flow phenomena and structure analysis. In vitro, velocity profiles, shear stresses, regurgitation, and energy losses determine the valve hemodynamics performance with respect to blood cell damage and thrombus formation.[1,2] Structural analysis ascertains the valve durability and leaflet failure mode, including stress/strain-related calcifications.

The limitations of existing artificial heart valves are well documented in the literature and a number of alternative designs have been suggested and have been hydrodynamically and structurally examined.[3,4] Although the results from these studies revealed satisfactory correlations between in vitro measurements and in vivo clinical and pathological findings, they still highlighted the need for biocompatible, hydrodynamically efficient, and cost-effective prosthetic heart valves. Hemodynamic studies of various valve designs, both experimentally and numerically, have been extensively carried out, with some of the research focusing on stress analysis and the dynamic structure of various prosthetic valves. These studies were thoroughly reviewed in the recent works of Morsi et al.[5,6] and Yoganathan et al.[7] In early structural analyses of aortic valves, leaflet models were based on the bending curvature of the leaflets caused by the pressure difference across the leaflet.

The emphasis of the aforementioned studies was either on the hydrodynamics or the stress analysis of the valve structure independently. However, it is essential to consider both the fluid and structural dynamics of the valve simultaneously for the valvular motion and the blood flow to be simulated correctly. This led to the inclusion of fluid–structure interaction (FSI) in the modeling of heart valve flow and was initially introduced by Peskin and McQueen,[8] who studied various mitral valves in a two-dimensional (2D) planar representation of the heart, including the left atrium and ventricle. The laminar, Newtonian, and Navier–Stokes equations were loosely coupled with equations defining the boundary forces and movements and constitute Peskin's immersed boundary technique. This method has been extended to simulate various valves and hearts.[9,10] The importance of FSI on the performance of heart valves was further highlighted by Makhijani et al.,[11] who developed a

Received: July 13, 2006 / Accepted: November 11, 2006

Y.S. Morsi (✉) · C.S. Wong · S. Das
Biomechanics and Tissue Engineering Group, Industrial Research Institute IRIS, Swinburne University of Technology, PO Box 218, Hawthorn, VIC 3122, Australia
Tel. +61-3-9214-8646; Fax +61-3-9214-5050
e-mail: ymorsi@swin.edu.au

W.W. Yang
Division of Minerals, Commonwealth Scientific and Industrial Research Organisation, Clayton, Victoria, Australia

three-dimensional (3D) coupled fluid–structure dynamics model for a generic pericardial aortic valve in a rigid aortic root graft. Blood flow was modeled as pulsatile, laminar, Newtonian, incompressible flow and the structure model accounted for material and geometric non-linearties. Finite volume computational fluid dynamics code and finite element structural dynamics code were coupled using an implicit "influence coefficient" technique. The computational predictions were in close agreement with corresponding in vitro experimental data.

The significance of the wall movement on the blood flow was also examined by Bathe and Kamm,[12] who used the finite element technique to model the pulsatile blood flow through a compliant stenotic artery. The fluid response was analyzed using an arbitrary Lagrangian–Eulerian (ALE) formulation for analyzing the fluid domain with moving boundaries for the artery structure. The finite element method (FEM) was used for the axisymetric modeling of both the fluid flow and the artery structure. Research by De Hart et al.[13] presented a fully coupled 3D model of an aortic heart valve using the Lagrange multiplier-based fictitious domain (FD) integrated within the FEM. The time-dependent physiological flow and aortic pressures were applied at the inflow and outflow plane, and the opening and closing configurations were demonstrated to be significantly different. This FD approach took into consideration the fact that the solid domain was immersed in the fluid domain with nonconformal meshes with respect to each other. Such an approach has been widely utilized, as shown by Baaijens and Glowinski et al.[14–16] and was successfully applied to a stentless valve by De Hart et al.[17]

The current understanding seems to indicate that during systole, the natural leaflet is subjected to a much lower stress than a mechanical or prosthetic leaflet. Moreover, unlike prosthetic valve membranes during systole, the natural leaflet is not subjected to compressive stresses during the cardiac cycle. Recent modeling of the induced stresses and the deformation of valve leaflets during coaptation and closure has been studied using FEM by incorporating shell and solid elements. Furthermore, two factors need to be taken into consideration: the interaction of the aorta wall with the valve membrane, which influences the flow patterns in the whole system, and the flexible structure of the leaflets. Note that the disk of a mechanical valve can be modeled as a rigid body because the stress and strain encountered is of less significance to such a value than to tissue valves with a flexible structure, for which the bending stiffness of the leaflet is very low compared to the tensile strength along the leaflet surface. In addition, the deformation of the leaflets results in large geometrical changes. During the deceleration phase (diastolic), the valve has to withstand the physiological transvalvular pressure gradient. These issues become challenging and increase in complexity when applied to 3D systems, such as the problem at hand.

The structure of the trileaflet valve being examined in this study is a typical example in which the motion of a thin-walled, leaflet-like structure is driven by the motion of the blood flow. The large deformation of the physical (structural) boundary due to the fluid forces and the nonlinearity of the material greatly increase the numerical difficulty. Such geometrically nonlinear structures are usually formulated in a Lagrangian description, while the fluid is often expressed in an Eulerian format due to the presence of convective terms. Note that the presence of convective terms in the case of moving boundary flow increases the numerical complexity in the Eulerian description, whereas the Lagrangian description for a structural moving boundary is simpler. Moreover, due to the large flow distortions and large structural deformations, element entanglement leads to the use of the ALE technique. This technique is now well recognized for the type of simulation in hand, which involves mesh generation over a considerable time span.[17] However, in cases of large deflections, interpolation techniques are required to update the variables for the newly generated mesh. The updated mesh may introduce an artificial diffusivity, which is a major concern regarding the applicability of ALE in some circumstances. Thus, a fictitious domain/mortar element (FD/ME) method has been proposed,[14] in which the fluid is described using a fixed mesh in an Eulerian setting with a Lagrangian formulation for the solid. In the FD method, the velocity constraint associated with the rigid internal boundaries is imposed by means of the Lagrange multiplier, while the ME method allows the coupling of domains with dissimilar element distributions.[18,19] The major advantage of the FD/ME method is that it does not require any updating of the mesh of the fluid domain. However, updating of the mesh becomes inevitable for very large deflections.

In this article, the development of a 3D transient coupled-fluid structure computational model of a trileaflet heart valve is presented. The overall aim was to examine the hydrodynamic behaviour of a partially opened thin leaflet valve, which plays an important role in the deformation and stresses of the flow, for various times and flow rates. A linear relationship between time and flow during the acceleration phase would enable the analysis at 50 μs to be extrapolated to the overall flow profiles.[20] Additionally, as the number of time steps increases, the computational analysis becomes laborious. Thus, the analysis was constrained to 50 μs. The ALE-coupled approach was used because it uses physically correct governing equations in the respective domains.

Materials and methods

The numerical approach

The present analysis was carried out in the ANSYS-FLOTRAN (Ansys Inc., South Point, USA) multiphysics environment and uses the sequential weak coupling method. The computational domains were separately defined as mathematical descriptions of the fluid domain (blood flow) and the solid domain (leaflets) and then coupled in an iterative sequential numerical algorithm. The leaflet motion was transiently updated by the solution of the leaflet domain, with the fluid domain solution providing fluid–structure interface loadings.

The equation(s) governing a viscous incompressible Newtonian fluid flow in the spatial domain with fixed spatial coordinates is as follows. Vector x (characteristic of the Eulerian formulation) in general scalar transport form is used, and Γ_ϕ and S_ϕ are the diffusion coefficient and the source term respectively:

$$\frac{\partial}{\partial t}(\rho\bar{\phi})+\frac{\partial}{\partial x}(\rho u\bar{\phi})+\frac{\partial}{\partial y}(\rho v\bar{\phi})+\frac{\partial}{\partial z}(\rho w\bar{\phi})= \frac{\partial}{\partial x}\left(\Gamma_\phi\frac{\partial\bar{\phi}}{\partial x}\right)+\frac{\partial}{\partial y}\left(\Gamma_\phi\frac{\partial\bar{\phi}}{\partial y}\right)+\frac{\partial}{\partial z}\left(\Gamma_\phi\frac{\partial\bar{\phi}}{\partial z}\right)+S_\phi \quad (1)$$

Equation 1 reduces to a continuity and momentum equation by substituting $\bar{\phi}=1$; $\Gamma_\phi=0$; $S_\phi=0$; and $\bar{\phi}=$ u, v, or w respectively.

The differential equation for homogeneous isotropic elastic structures, a material domain with material coordinates vector X, is employed in a Langrangian description:

$$\rho_w\frac{d^2d_i}{dt^2}=\tau_{ij,j}+F_i \quad (2)$$

where d_i and ρ are the displacement vector and density of the elastic medium, respectively, and $\tau_{ij,j}$ and F_i are shear stress and forces, respectively.

For the ALE description, a referential domain, with grid/mesh coordinate vector χ is used. The spatial coordinate x can be expressed as a function of material coordinates, mesh coordinates, and time as:

$$x=f(x(X,t)); \quad x=f(x(\chi,t)) \quad (3)$$

The equations of Eq. 3 are the basis for obtaining the relationship between these three domains for ALE formulation. By differentiating the material and mesh coordinates with respect to time t, the material and mesh velocities can be obtained as:

$$v=\left.\frac{\partial x(X,t)}{\partial t}\right|_X; \quad \hat{v}=\left.\frac{\partial x(\chi,t)}{\partial t}\right|_\chi \quad (4)$$

The difference between this material velocity and the reference (mesh) velocity defines the convective velocity. Thus, the material time derivative of a passive scalar ϕ at a given point χ_i in the fluid domain at time t can be expressed as follows:

$$\frac{D\phi(\chi_i,t)}{Dt}=\frac{\delta\phi(\chi_i,t)}{\delta t}+(v-\hat{v})\frac{\delta\phi(x_i,t)}{\delta x_i} \quad (5)$$

Substituting Eq. 5 into the unsteady convection–diffusion transport equation for ϕ in the Lagrangian description, we can obtain the following equation:

$$\phi_t+(u-\hat{v}_1)\phi_x+(v-\hat{v}_2)\phi_y+(w-\hat{v}_3)\phi_z +-\frac{\mu}{\rho}(\phi_{xx}+\phi_{yy}+\phi_{zz})=0 \quad (6)$$

The reference velocity $\hat{v}$ can be chosen arbitrarily. If $\hat{v}$ is equal to zero, the above transport equation for ϕ becomes an equation in the Eulerian description. Therefore, the conservation equations (continuity and momentum equations) for the fixed grid can be transformed to their respective moving grids by using the moving grid velocity vector:

$$u_x+v_y+w_z=0 \quad (7)$$

$$u_t+(u-u_g)u_x+(v-v_g)u_y+(w-w_g)u_z =-\frac{1}{\rho}p_x+\frac{\mu}{\rho}(u_{xx}+u_{yy}+u_{zz}) \quad (8)$$

$$v_t+(u-u_g)v_x+(v-v_g)v_y+(w-w_g)v_z =-\frac{1}{\rho}p_y+\frac{\mu}{\rho}(v_{xx}+v_{yy}+v_{zz}) \quad (9)$$

$$w_t+(u-u_g)w_x+(v-v_g)w_y+(w-w_g)w_z =-\frac{1}{\rho}p_z+\frac{\mu}{\rho}(w_{xx}+w_{yy}+w_{zz}) \quad (10)$$

By substituting Eq. 2 in the above Eqs. 7–10, the Navier equation for elastic material was obtained. Thus, the Navier–Stokes equations and the continuity equation with elastic materials are solved iteratively. A complete and detailed description of the ALE formulation can be found in Huerta and Liu.[21]

Problem definition

Although the localized turbulence at the initial opening of the valve can have an effect on the local shear stress and fluid flow in general, for the time steps considered here (0.02 s) the effect is consider to be negligible, and only laminar, Newtonian, incompressible flow was considered in this study.

Figure 1a shows a schematic representation of a trileaflet valve inside a straight tube with an outer diameter of 26 mm. The fluid domain started at 2D upstream of the valve (Y = –58 mm) and ended at 1D downstream of the valve (Y = 26 mm); the origin of the Y-axis was at the bottom of the valve. As the simulation was carried out based on the assumption of a rigid wall, a Dirichlet boundary condition was applied throughout the structure, including parts that were joined to the wall. A uniform velocity was specified at the inlet with zero pressure assumed at the outlet. Moreover, at the fluid–structure interface, the instantaneous pressure was transferred from the fluid solution to the structural solution sequentially as the solution proceeded.

The geometry of the trileaflet valve was chosen based on the design produced by Jiang et al.[22] and the free form surface of a leaflet with a thickness of 0.35 mm was created using B-splines, as described in Penrose and Staples.[23] The valve was placed in a straight duct without sinuses for simplification of the model and the leaflet thickness was chosen to accommodate the limitations of thin structures in the FSI analysis. As shown in Fig. 1b, the valve leaflets were made of polyurethane material with the properties of density, ρ = 954 kg/m^3; elasticity modulus, E = 0.5 GPa; and a Poisson's ratio of 0.49. The material was considered isotropic and linearly elastic. The blood analog fluid had a kinematic viscosity of 3.5 cSt.

The finite element discretization of the fluid domain was carried out with tetrahedral elements (Fig. 2a), while hexahedral elements (brick meshing) were used for the discretization of the valve structural components, as shown

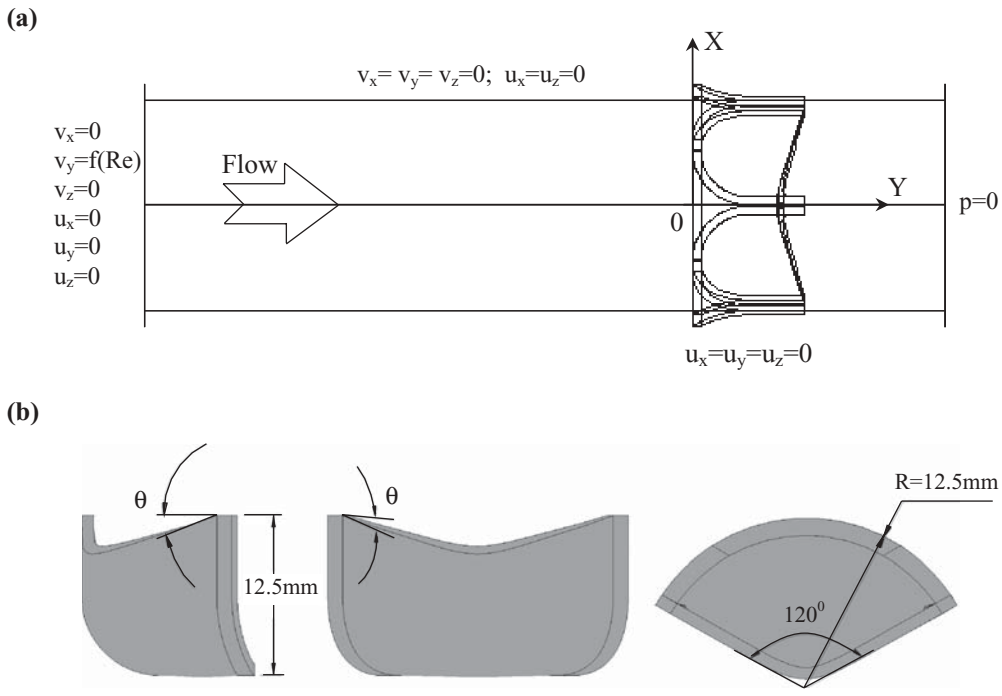

Fig. 1a,b. Schematic of a trileaflet heart valve. **a** Boundary conditions, **b** leaflet details (θ is chosen arbitrarily)

in Fig. 2b. In this study, the fluid and solid mesh were assumed to be dissimilar along the fluid–leaflet interface, which meant that the nodes of the fluid and the structural domain did not coincide spatially along the interface. Hence, a sequential weak coupling method was adopted, where the load was transferred across a dissimilar mesh by using a nonconservative interpolation technique. Depending on the intersections of the solids with the fluid mesh, fluid elements were either reshaped or added. Grid dependence studies were carried out to optimise the CPU time and the constituency and the accuracy of the results. The convergence criterion was less than 1%. All numerical simulations were performed using the commercial software package, ANSYS.

Results

Since this study was concerned with the initial period of valve opening, only the results relating to the initial time steps, i.e., from 0 to 0.05 s, are presented here. Therefore, only low Reynolds numbers ranging from 100 to 600 were considered and the corresponding blood flow rate varied from 0.445 to 2.67 l/min, respectively. Based on the experimental conditions, laminar, Newtonian, incompressible flow was considered in the analysis. The results are presented in terms of the axial velocity profiles along the valve and the wall shear stress distributions in the vicinity of the leaflets under the above-mentioned flow and time conditions.

Axial velocity distributions

Figure 3 shows the geometrical views of the initial valve opening at three times for a Reynolds number of 100. It can be clearly seen that the open area of the valve orifice increased significantly between 0.01 and 0.03 s. However, a less pronounced increase in the open area was observed for the later time step 0.03–0.05 s. Furthermore, a symmetrical wavy structure was formed at the tip of each leaflet at the initial opening stages, which suggests that the leaflet was subjects to both compressive and tensile stresses on both sides of the leaflet.

Figure 4 presents data which demonstrate the axial velocity, V_y, profiles along the centerline of the tube for all the Reynolds numbers investigated at different times (t = 0.01–0.05 s). Two vertical grid lines at Y = 0 mm and Y = 9 mm indicate the central distance between the bottom and the tip of the leaflet, respectively. Figure 4 shows that as the flow approached the entrance of the valve, the axial velocity increased rapidly toward the exit of the valve due to the restraints of the orifice opening area at the tips of the leaflets. All profiles indicate that the axial flow velocity reached its peak just after the valve exit for all Reynolds numbers and times investigated. Moreover, as expected, the peak axial velocity increased significantly as the Reynolds number increased from 100 to 600. On the other hand, for a constant Reynolds number, the axial velocity reached its peak between 0.03 and 0.04 s, and then decreased at 0.05 s, which indicated the further opening of the valve orifice area as time progressed. It was also evident that the gradient of the axial velocity deceleration downstream of the valve

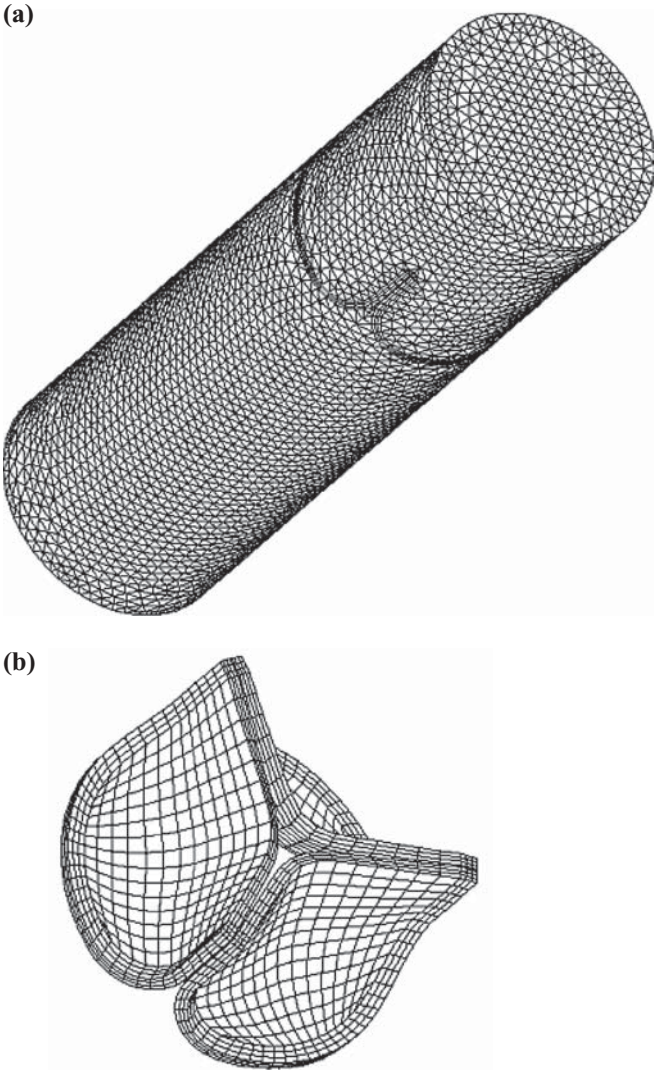

Fig. 2a,b. Fluid domain and valve structure discretization. **a** Tetrahedral elements were used for the fluid domain and **b** hexahedral elements for the valve structure

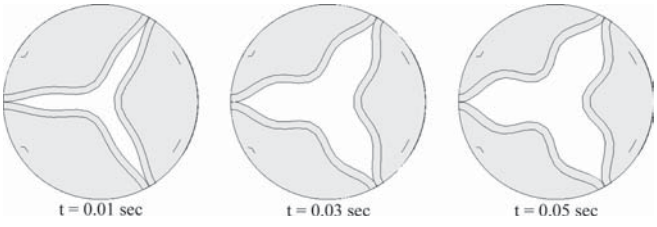

Fig. 3. Valve opening at initial loading stages based on a Reynolds number of 100

decreased significantly with increasing time and Reynolds number. The above results and general trends are consistent with the experimental findings of Woo et al.[24]

In Fig. 5, 2D velocity, V_x and V_y, vectors are plotted in the symmetrical plane across the tube length at three times for a Reynolds number of 600. The velocity vector length was scaled to three times the original length to clarify the flow fields. It was apparent that the region behind the leaflet near the wall of the valve contained very low reversal velocities, which was the main factor in the development of a potential recirculation zone. The flow of this region was essentially laminar and concentrated around the underside of the leaflet. The center of this circulation tended to move toward the tip of the leaflet as the time increased. The majority of the flow was observed around the body of the leaflet, dissipating as it reached the tip. Additionally, the flow became detached from the leaflet over time and this detachment pushed the circulation zone further downstream. The circulation zone on the topside of the leaflet increased in intensity as the time (opening) increased. Similar observations were reported by Stevenson and Yoganathan.[25] However, as observed in Figure 5, the reversal flow diminished as the flow progressed further downstream of the valve, a phenomenon that was not observed by Stevenson and Yoganathan.[25]

Wall shear stress distribution

The magnitude and distribution of the shear stresses depended mainly on the size, shape, and orientation of the valve leaflets. Figure 6 shows the wall shear stress distribution along the vertical central line, h, of the leaflet for different Reynolds numbers at a time of 0.05 s. It was observed that the wall shear stress increased gradually from the base of the leaflet toward the tip, and reached its peak at approximately 1 mm before the edge of the leaflet tip, where the maximum axial flow acceleration occurred. The peak wall shear stress on the leaflet increased almost 900% as the Reynolds number increased from 100 to 600, as shown in Fig. 6.

Figure 7 shows the wall shear stress distribution along the vertical central line, h, of the leaflet at different times for a constant Reynolds number of 600. The peak wall shear stress increased as the time increased, reaching its maximum at a time of 0.03 s. Note that a similar trend was observed for the axial velocity profiles along the centerline of the valve (see Fig. 4). The increase in peak wall shear stress at different times for a Reynolds number of 600 was approximately 130%. This shear stress effect became significantly less as the Reynolds number increased.

Since a horizontal wavy structure formed in the leaflet during the initial opening of the valve (Fig. 3), it was necessary to investigate the wall shear stress along different horizontal cross sections of the leaflet. Figure 8 demonstrates the wall shear stress distributions along the horizontal span, S, of the leaflet at four horizontal cross sections, A, B, C, and D respectively. The vertical grid line at S = 0 mm indicates the location of vertical centerline of the leaflet. The conditions were a time of 0.05 s and a Reynolds number of 600. It can be seen that the maximum wall shear stress appeared at the top horizontal section, D, toward the two sides of the leaflet. This was mainly caused by the restraining of the orifice opening area near the sides of the leaflet where the maximum axial velocity gradient occurred. At section D, the maximum wall shear stress magnitude of 40 N/m^2 was approximately 3.5 times higher than that at the

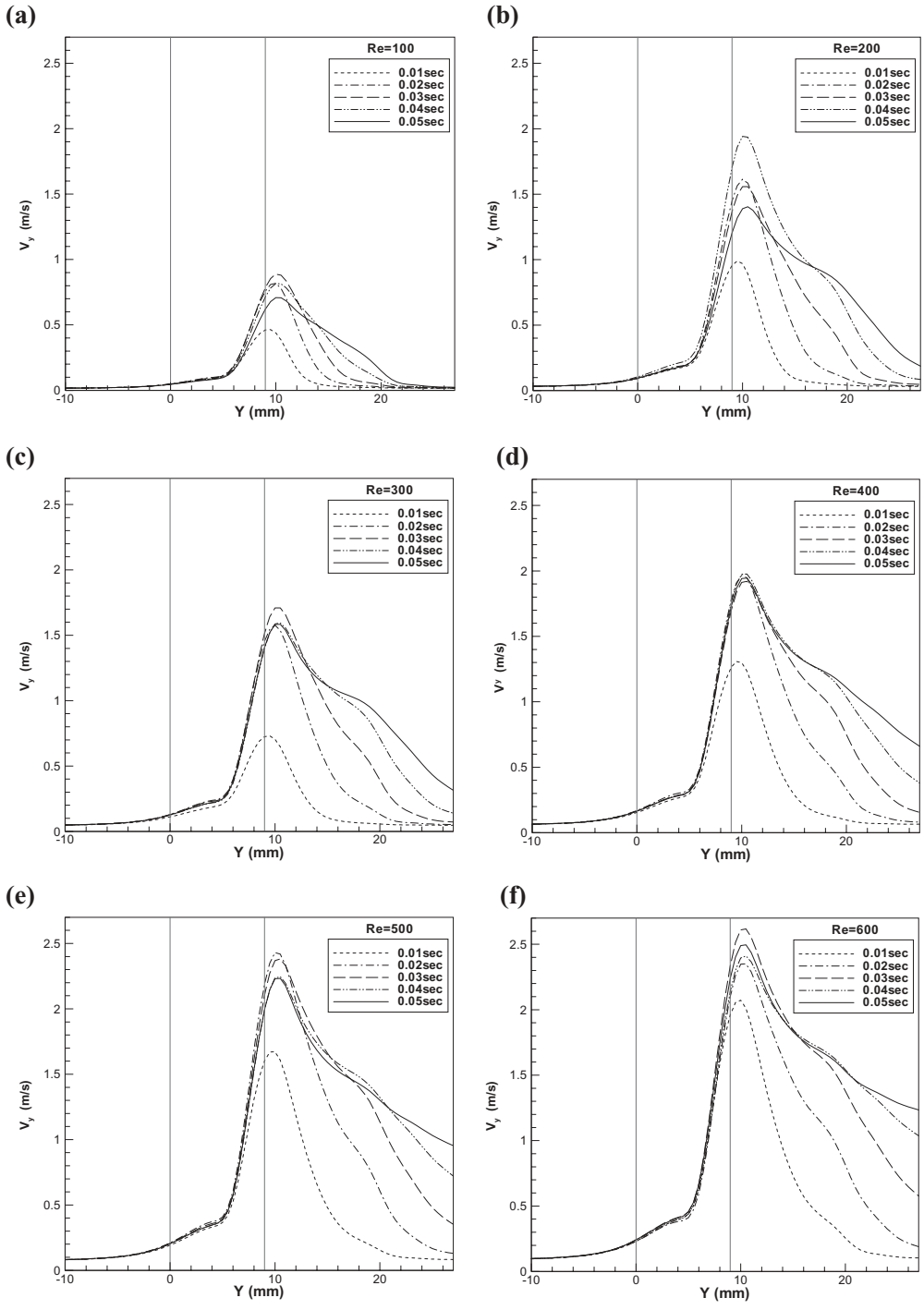

Fig. 4. Axial velocity (V_y) profiles along the centerline at various initial time steps and Reynolds numbers (Re) of **a** 100, **b** 200, **c** 300, **d** 400, **e** 500, and **f** 600

vertical centerline. It was expected that the wall shear stress would increase significantly as the horizontal level increased toward the tip of the leaflet.

The wall shear stress distribution along horizontal cross section D at different times is presented in Fig. 9, in which the Reynolds number was 600. Small changes in wall shear stress were observed at different times with approximately 40% variations in magnitude. This was also an indication that the valve was still in the initial opening stages, and there was no significant change with respect to the deformation of the leaflet.

Discussion

The existence of large pressure gradients during the short duration of the opening phase may induce high-velocity flow through the orifice opening, as shown by the results of the present study. Hence, if the valve did not open or respond to the fluid force during the opening phase, this would lead to higher axial velocity gradients which may result in higher wall shear stresses. The maximum wall shear stress was expected to occur during the opening phase

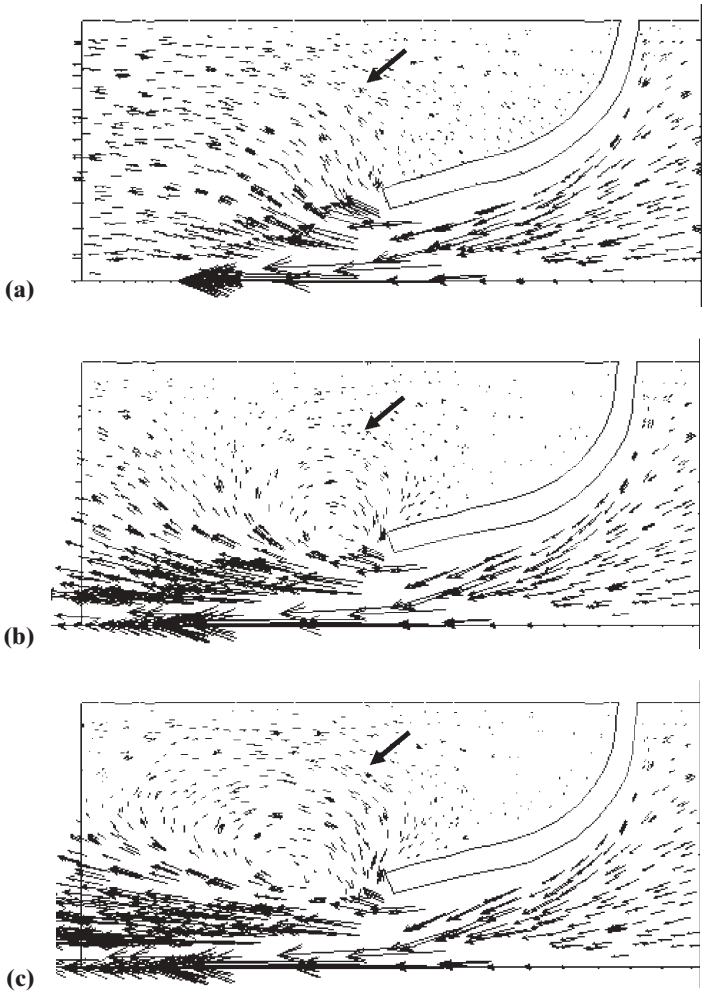

Fig. 5. Velocity vectors around a leaflet at a Reynolds number of 600 and various initial time steps (**a** 0.01, **b** 0.03, and **c** 0.05 s)

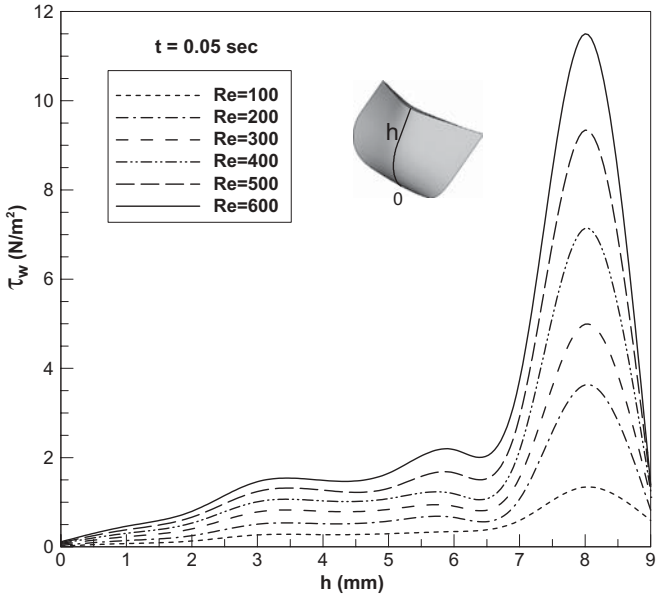

Fig. 6. Wall shear stress (τ_w) distributions along the middle vertical line of a leaflet at 0.05 s and various Reynolds numbers ranging from 100 to 600. *h*, vertical centerline

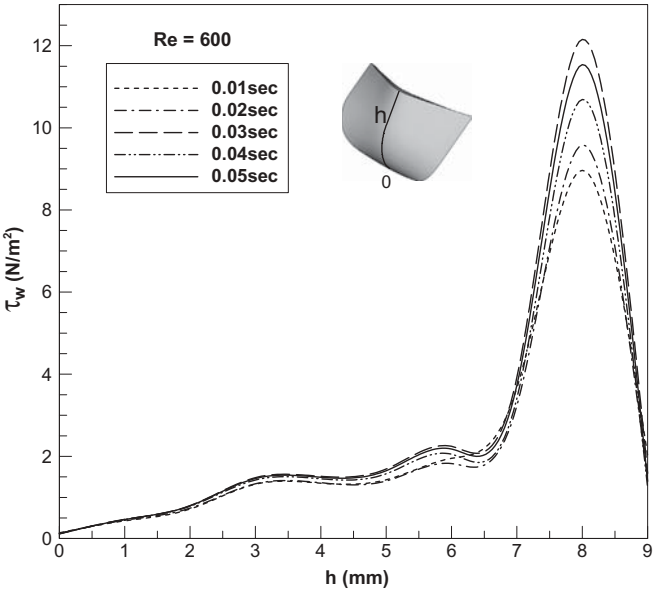

Fig. 7. Wall shear stress distributions along the middle vertical line of a leaflet using a Reynolds number of 600 at various initial time steps ranging from 0.01 to 0.05 s

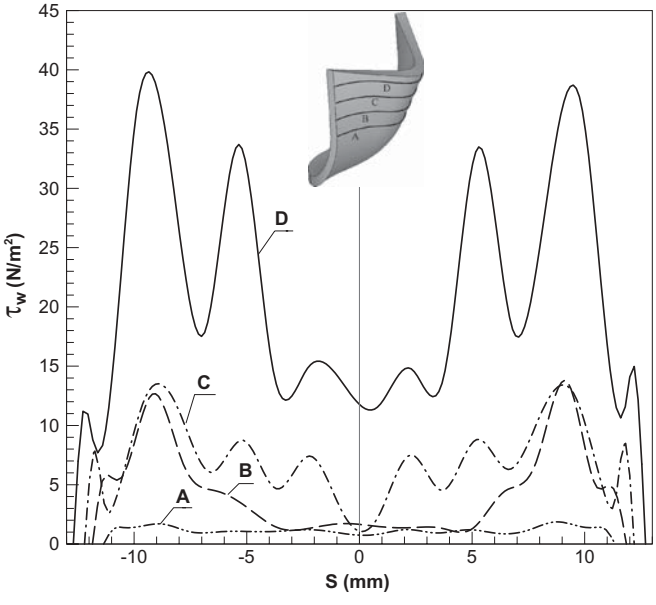

Fig. 8. Wall shear stress profiles across horizontal sections of the leaflet (*A*–*D*) at 0.05 s and a Reynolds number of 600. *S*, the horizontal span of the leaflet

because of the reduced orifice area. The same reasoning applies during the closing of the valve, and various other researchers have reported the existence of high wall stresses during the closing period.[17,25] Thus, the higher wall shear stresses which cause platelet activation and subsequent thrombus initiation may be associated with the opening phase as well as the closing phase.

On the other hand, it was recognized that a fast response from the structural parts (i.e., the valve) could reduce these stresses to a large extent. The fluid forces together with

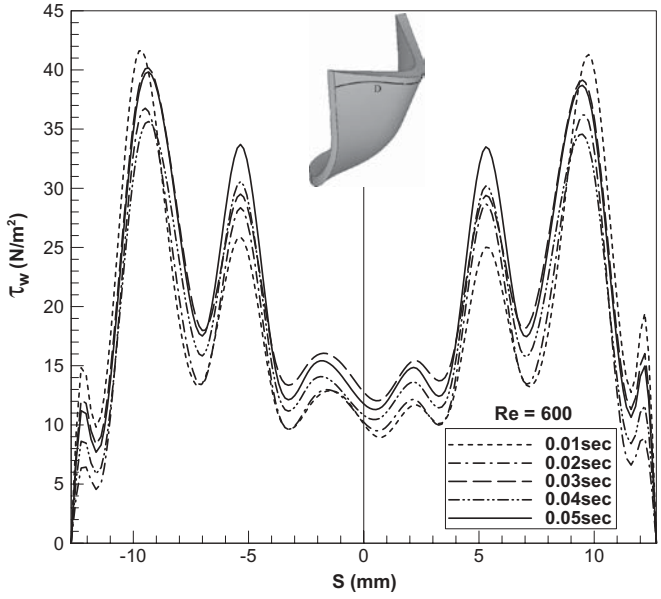

Fig. 9. Wall shear stress profiles across horizontal section D of a leaflet at initial times of 0.01–0.05 s and a Reynolds number of 600

structural deflection could play a major role in influencing the initial value of the wall shear stress and the velocity gradient near the solid structure. The wavy structure of the leaflet resulted in a concentration of shear stress at the top corners of each leaflet at the opening stage of the valve. This stress concentration reduced with increasing time (Fig. 8), highlighting the importance of understanding the development of these stresses from the initial time (t = 0.01 s) so that the fatigue behavior of the leaflet can be analyzed. A comparison of different Reynolds numbers (Re = 100–600, i.e., 0.445–2.67 l/min) showed that the trends of shear stress development were similar over this range of Reynolds numbers and over the leaflet profile and can be as high as 40 N/m^2 for a Reynolds number of 600.

Conclusions

The ALE technique was successfully applied to a 3D problem involving fluid–structure interactions typically found in cardiovascular applications. Specifically, we demonstrated the capability to model the coupled behavior of a leaflet behaving as an elastic solid with an incompressible fluid. Although few data were available for validation, confidence in the current results was gained through qualitative comparison with our previous experimental results.[6] The results presented in this study clearly showed complex stress development patterns during the initial opening of the valve, which is considered to be the most detrimental factor for fatigue failure analysis. It is anticipated that the results from such simulations will provide invaluable information for the design of leaflets of prosthetic heart valves.

Acknowledgment This research was supported by the Australian Research Council Discovery Scheme.

References

1. Baldwin JT, Tarbell JM. Mean velocities and Reynolds stresses within regurgitant jets produced by tilting disc valves. ASAIO Trans 1991;37:348–349
2. Sakhaeimanesh AA, Morsi YS. Analysis of regurgitation, mean systolic pressure drop and energy losses for two artificial aortic valves. J Med Eng Tech 1999;22(2):63–68
3. Reul H, Potthast K. Durability/wear testing of heart valve substitutes. J Heart Valve Dis 1998;7(2):151–157
4. Lin Q, Morsi YS, Smith B, Yang W. Numerical simulation and structure verification of jellyfish heart valve. Int J Comput Appl Tech 2004;21:2–7
5. Morsi YS, Birchall IE, Rosenfeldt FL. Artificial aortic valves: an overview. Int J Artif Organs 2004;27:445–451
6. Morsi YS, Birchall IE. Tissue engineering a functional aortic heart valve: an appraisal. Future Cardiol 2005;1(3):405–411
7. Yoganathan AP, He Z, Jones SC. Fluid mechanics of heart valves. Annu Rev Biomed Eng 2004;6:331–362
8. Peskin CS, McQueen DM. Modelling prosthetic heart valves for numerical analysis of blood flow in the heart. J Comput Phys 1980;37:113–132
9. Peskin CS, McQueen DM. Fluid dynamics of the heart and its valves. In: Othmer HG, Adler FR, Lewis MA, Dallon JC (eds) Case studies in mathematical modeling – ecology, physiology, and cell biology. Englewood Cliffs: Prentice-Hall, 1996;309–337
10. Peskin CS. The immersed boundary methods. Acta Numer 2002; 11:479–517
11. Makhijani VB, Yang HQ, Dionne PJ, Thubrikar MJ. Three-dimensional coupled fluid–structure simulation of pericardial bioprosthetic aortic valve function. ASAIO J 1997;43:387–392
12. Bathe M, Kamm RD. A fluid–structure interaction finite element analysis of pulsatile blood flow through a compliant stenotic artery. J Biomech Eng 1999;121:361–369
13. De Hart J, Peters GWM, Schreurs PJG, Baaijens FPT. A three-dimensional analysis of fluid–structure interaction in the aortic valve. J Biomech 2003;36:103–112
14. Baaijens FPT. A fictitious domain/mortar element method for fluid–structure interaction. Int J Numer Method Fluids 2001;35: 743–761
15. Glowinski R, Pan TW, Periaux J. A Largrange multiplier/fictitious domain method for the numerical simulation of incompressible flow around moving rigid bodies: (I) case where the rigid body motions are known a priori. Comptes Rendus de I'Academie des Sciences Series I Mathematics 1997;325:783–791
16. Glowinski R. Finite element for incompressible viscous flow. In: Ciarlet PG, Lion JL (eds) Handbook of numerical analysis, vol IX. Amsterdam: North-Holland, 2003
17. De Hart J, Baaijens FPT, Peters GWM, Schreurs PJG. A computational fluid–structure interaction analysis of a fiber-reinforced stentless aortic valve. J Biomech 2003;63:699–712
18. Donea J. An arbitrary Lagrangian–Eulerian finite element method for transient fluid–structure interactions. Comput Methods Appl Mech Eng 1981;33:689–723
19. Bertrand F, Tanguy PA, Thibault F. A three-dimensional fictitious domain method for incompressible fluid flow problems. Int J Numer Methods Fluids 1997;25:719–736
20. Morsi YS, Sakhaeimanesh AA. Flow characteristics past jellyfish and St. Vincent valves in the aortic position under physiological pulsatile flow conditions. Artif Organs 2000;24:564–574
21. Huerta A, Liu WK. Viscous flow with large free surface motion. Comput Methods Appl Mech Eng 1988;69:277–324
22. Jiang H, Campbell G, Boughner D, Wan WK, Quantz M. Design and manufacture of polyvinyl alcohol (PVA) cryogel tri-leaflet heart valve prosthesis. Med Eng Phys 2004;26:269–277
23. Penrose JMT, Staples CJ. Implicit fluid–structure coupling for simulation of cardiovascular problems. Int J Numer Methods Fluids 2002;40:467–478
24. Woo YR, Williams FP, Yoganathan AP. Steady and pulsatile flow studies on a trileaflet heart valve prosthesis, Scand J Thorac Cardiovasc Surg 1983;17:227–236
25. Stevenson DM, Yoganathan AP. Numerical simulation of steady turbulent flow through trileaflet aortic heart valves-I. Computational scheme and methodology. J Biomech 1985;18:899–907